ChemSusChem

Research Article
doi.org/10.1002/cssc.202300585

Chemistry Europe
European Chemical Societies Publishing

www.chemsuschem.org

VIP *Very Important Paper*

Green Additives in Chitosan-Based Bioplastic Films: Physical, Mechanical, and Chemical Properties

Kordula B. Schnabl[+],[a] Laurens D. B. Mandemaker[+],[a] Klaas G. J. Nierop,[b] Olivier V. B. Deen,[a] Desmond D. Eefting,[b] Ina Vollmer,[a] and Bert M. Weckhuysen*[a]

To switch to alternatives for fossil-fuel-based polymer materials, renewable raw materials from green resources should be utilized. Chitosan is such a material that is a strong, but workable derivative from chitin, obtained from crustaceans. However, various applications ask for specific plastic properties, such as certain flexibility, hardness and transparency. With different additives, also obtainable from green resources, chitosan-based composites in the form of self-supporting films, ranging from very hard and brittle to soft and flexible were successfully produced. The additives turned out to belong to one of three categories, namely linear, non-linear, or cross-linking additives. The non-linear additives could only be taken up to a certain relative amount, whereas the uptake of linear additives was not limited within the range of our experiments. Additives with multiple functional groups tend to crosslink chitosan even at room temperature in an acidic medium. Finally, it was shown that dissolving the chitosan in acetic acid and subsequently drying the matrix as a film results in reacetylation compared to the starting chitosan source, resulting in a harder material. With these findings, it is possible to tune the properties of chitosan-based polymer materials, making a big step towards application of this renewable polymer within consumer goods.

Introduction

In a world with a steadily growing population, the need to satisfy the increasing demands in energy and materials is a complex challenge.[1] Opposite to this growing demand, many of Earth's resources, like for instance the readily available fossil fuels, are gradually diminishing. A prominent example that still heavily relies on fossil feedstocks is the production of polymers, including coatings and plastics. During the Second World War, fossil feedstocks were increasingly used for synthetic plastic production to overcome the scarcity of natural polymers, such as rubber.[2] Due to its easy, large-scale production, the volume of synthetic plastic has increased from 2 million metric tons per year in 1950 to 368 million metric tons per year in 2019, as its essentiality is increasing massively.[3,4] With growing demand and production, the subsequent pollution caused by plastics became a serious environmental problem, which resulted in a campaign to eliminate single-use plastic usage by 2022 of the United Nations Environment Program.

Inevitably, since unsustainable fossil resources are not inexhaustible, a shift towards renewable sources, such as agricultural and municipal waste, and recycling techniques must take place. Different technologies, which enable the reuse and valorisation of plastic waste products, already demonstrate a big impact, but their proceeding evolution/advancement is still of paramount importance.[5] However, the use of fossil fuels cannot be replaced by a single alternative, which sparks the need to valorise different resources to gradually reduce the dependence on fossil fuels.[5,6] Therefore, the future focus of research should lay on two different aspects: firstly, the recycling and valorisation of already used plastic products, which helps to avoid waste production that harms the environment and further enables the formation of new chemical building blocks or materials for different purposes,[7] and secondly, the discovery of alternative, renewable materials, which can be used for plastic production, like for example natural polymers.[1,8]

Natural polymers often have the benefit of being biodegradable, which simplifies the handling of the waste and simultaneously reduces harmful impacts on the environment.[8,9] Furthermore, its non-toxic property stands in contrast to its counterparts derived from petrochemicals. In earlier research, polysaccharides showed to be an ideal feedstock for multiple applications.[8,10] The seek for alternatives is therefore at its peak, giving renewable biopolymers occurring in living organisms and biodegradable substances a helpful application.[9,11]

One of such biopolymers is chitin, which, after cellulose, is the second most abundant polysaccharide in the world.[12] It consists of 2-acetamino-2-deoxy-D-glucose units, connected by

[a] *K. B. Schnabl,[+] Dr. L. D. B. Mandemaker,[+] O. V. B. Deen, Dr. I. Vollmer, Prof. Dr. B. M. Weckhuysen*
Inorganic Chemistry and Catalysis Group
Debye Institute for Nanomaterials Science and Institute for Sustainable and Circular Chemistry, Utrecht University
Universiteitsweg 99, 3584 CG Utrecht (The Netherlands)
E-mail: b.m.weckhuysen@uu.nl

[b] *Dr. K. G. J. Nierop, D. D. Eefting*
GeoLab, Faculty of Geosciences
Utrecht University
Princetonlaan 8, 3584 CB Utrecht (The Netherlands)

[+] *These authors contributed equally to this work.*

Supporting information for this article is available on the WWW under https://doi.org/10.1002/cssc.202300585

β-(1→4)-glycosidic-bonds. It can be found in the exoskeleton of arthropods, in the cell walls of fungi and yeast, in insect cuticles or marine animals, as reinforcement and giving strength.[12,13] As a waste material it is mainly derived from by-products of the fishing industry, where it is extracted predominantly from the exoskeletons of marine crustaceans, shrimps, lobsters, and crabs, but recently advances are also made to extract it from waste of mushroom farms, where the amount of waste ranges between 5% and 20% of the production volume.[12–15] Annually, around 100 billion tons of chitin are produced from living organisms in the ocean alone.[16] The remains of this source would provide a huge amount of crude material if proper commercial procedures for the extraction of commercially competent polymers would be developed. But despite recent advances are aiming to develop even green and eco-friendly approaches for the extraction of chitin and chitosan, it remains underutilized and is handled as a waste product by burning, landfilling, and dumping into the sea.[17,18]

Arguably, the insoluble character of the chitin bio-polymer limits its commercial applications. Therefore, different chitin derivates, chitosan being the most abundant one, are used.[12,19] Chitosan is produced by partial deacetylation of chitin on a commercial scale, attaining a degree of acetylation lower than 50%. This change in functionality enables chitosan to be soluble in acidic aqueous media, which promotes its use for different applications, mostly in composite materials.[12,19,20] The abundant derivate chitosan is renewable and has good thermal and chemical stability.[8,10,21] The presence of its diverse chemical functionalities, *e.g.*, amino groups, allows for an easy functionalization. This makes it possible to finetune its properties, as the exact molecular structure determines the polymer's characteristics, such as stiffness, strength, elasticity, and toughness.[1,10] Furthermore, chitosan is, as chitin and cellulose, listed in the Environmentally Degradable Plastic List (EDP).[22] With these properties, it is not surprising that it is one of the most studied polysaccharides, with about 20,000 articles published just on its applications as film materials since 2016.[23] Moreover, chitosan is already in successful use in commercially available biomaterials as a composite material in the medical sector, such as Beschitin W (Unitika, Japan)[24] or Excel Arrest (LCC Hemostatis Co, USA).[25]

Still, chitosan-based materials have not yet been used in product applications on a large scale as they cannot keep up with the various properties of established synthetic polymers.[26] With the right additives, such as plasticizers, chitosan polymers may meet the required properties and develop into an alternative for fossil fuel-based plastics in the new, sustainable society.[27–29] According to IUPAC, plasticizers are substances incorporated into a material (usually a plastic or elastomer) to increase its flexibility, workability, or distensibility.[30] But as an important aim of the studied chitosan materials is to diminish waste production, the additives should be biodegradable as well. In the past, the influence of a few biodegradable additives was already investigated on chitosan films. While glycerol and tween 20 were already investigated as a potential plasticizer especially for edible films and coatings[31] as well as for cinnamyl chitosan composite materials,[32] tween 80 was tested as a surfactant in drug delivery precursor mixtures of low molecular-weight chitosan.[33] This emphasizes the high interest and potential in the utilization of biobased additives, although research on a broader set of their characteristics is missing in order to understand their full potential.

To address this, and to provide a comprehensive comparison to select the best-fitting additive for each application, we investigated seven common, mostly biodegradable additives on their properties when added to chitosan to form films, as can be schematically seen in Figure 1. The studied additives are glycerol (GLY),[34–36] sorbitol (SOR),[35–38] polyethylene glycol (PEG),[28,36,39,40] lactic acid (LAC),[36] citric acid (CA),[36,41] Tween 20 (T20),[32,35] and Tween 80 (T80),[35,42] whose structure is depicted in Figure S1. The hardness and flexibility of the resulting films, as well as the interaction between the plasticizers and the chitosan, has been investigated. For the film synthesis, a commonly used route described by Arzate-Vazquez et al. was used,[43] with the addition of the additives with ratios of 0.5/1 up to 8/1 (additive/chitosan). It is obvious that these high amounts cannot be seen as "additive" anymore but were used by us to accentuate the differences between and the possibilities of the individual additives, and also to thoroughly investigate the uptake behaviour of them. The uptake and interaction behaviour were studied using attenuated total reflection-infrared (ATR-IR) spectroscopy and Pyrolysis gas chromatography coupled to mass spectrometry (Py-GC-MS). The films were then further examined with Grazing-Incidence X-Ray Diffraction (GI-XRD) to study the potential semi-crystallinity, if any. The mechanical properties of the materials made were assessed using atomic force microscopy (AFM), and more specifically quantitative nanomechanical mapping (QNM). We show that both the type of additive and its amount in a chitosan film can tailor the properties from transparent flexible, soft films (potentially applicable as e.g., cling film) to opaque, strong and dense films (potentially applicable as e.g., packaging material), and that a broad spectrum of properties can be achieved with the assessed additives.

Results and Discussion

When cast with acetic acid, chitosan-based films were showing a flat, mostly opaque film, with hardly any rips, air bubbles, or discolouring. For comparison, the films were also prepared with HCl as acidic source, as well as dried at elevated temperatures (i.e., 60 and 90 °C), which resulted in ripped or damaged films with yellow to brown coloured features (see Figure S2 for optical microscopy images). For a first observation on the optical properties of the films produced with the seven additives, round films were cast with an additive/chitosan ratio of 1/1 (wt/wt) and investigated with optical microscopy, as shown in Figure S3. A first impression on their flexibility, stability, and stiffness, was received by casting the same (1/1 ratio) mixtures in crab-shaped moulds, as shown in Figure 2. As apparent already by eye, the resulting films and shapes vary greatly in several ways. The pure chitosan film and the films formed with the addition of SOR, GLY, and PEG show the

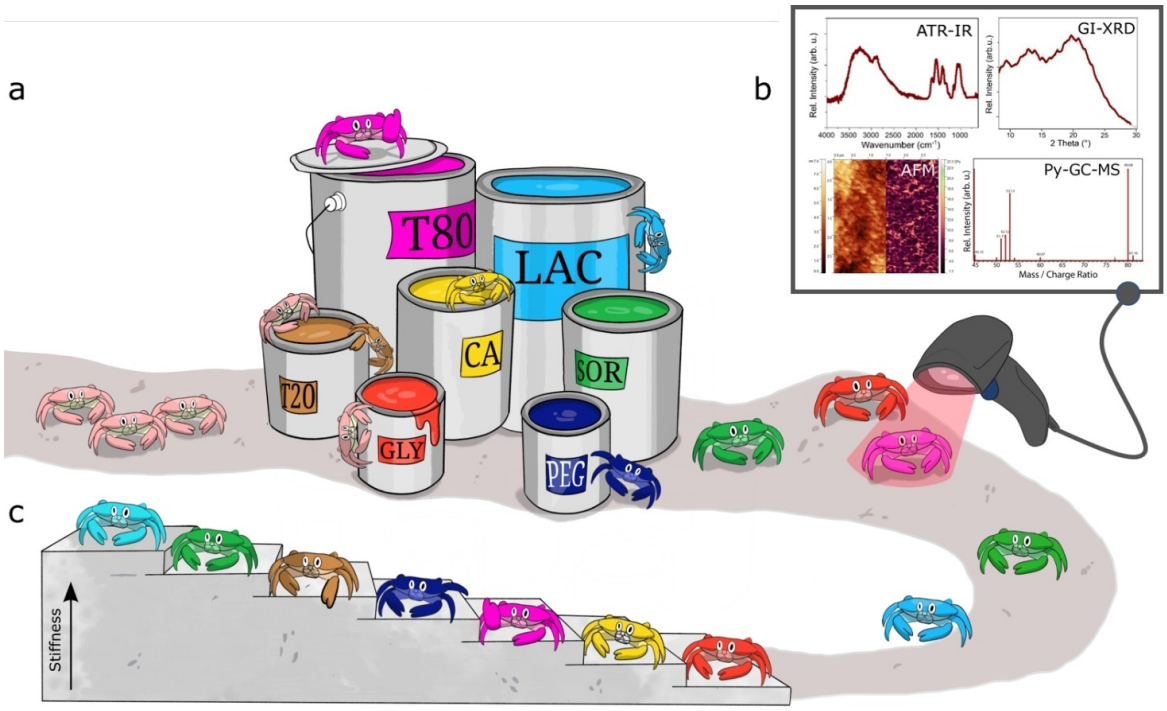

Figure 1. a) Schematic representation of the formation of chitosan films (indicated by crabs) with the addition of the additives glycerol (GLY; red), polyethylene glycol (PEG; dark blue), sorbitol (SOR; green), Tween 20 (T20; orange), Tween 80 (T80; violet), lactic acid (LA; light blue), and citric acid (CA; yellow). After drop casting and drying the mixtures, the films were analysed with techniques represented here with the spectra of pure chitosan for clarity. b) For attenuated total reflection infrared (ATR-IR) spectroscopy, all the spectra were normalized on the chitosan-specific N–H bend at 1550 cm^{-1} before the relative amounts of additive to chitosan were calculated. Pyrolysis gas chromatography coupled to mass spectrometry (Py-GC-MS) was used to confirm the found insights on the uptake behaviour of the additives. PeakForce quantitative nanomechanical mapping (QNM) was done using atomic force microscopy (AFM) and utilized to analyse the local DMT modulus, as well as surface homogeneity and roughness of the formed material. Finally, Gracing-Incidence X-Ray Diffraction (GI-XRD) was used to look at the crystalline properties of the formed films with respect to different additives. c) The final films with a 1/1 ratio of additive to chitosan were finally lined up with increasing stiffness.

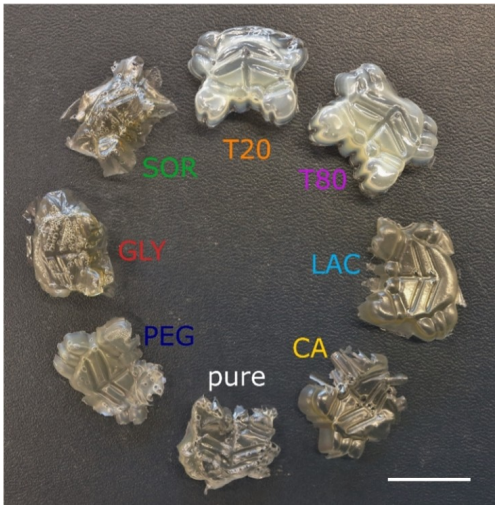

Figure 2. Crabs made of chitosan with different additives in the ratio 1/1. The abbreviations and colours indicated here will be used throughout this whole manuscript. As can be seen by eye, the tween 20 (T20; orange), tween 80 (T80; violet), lactic acid (LA; light blue), and citric acid (CA; yellow) resulted in smooth, whole products. In contrast, the pure chitosan (pure; white), polyethylene glycol (PEG; dark blue), glycerol (GLY; red) and sorbitol (SOR; green) resulted in broken crabs with bubble formation. In terms of hardness, T20, T80, PEG, SOR, and the pure, contained a harder structure, while the crabs made with LA, CA, and GLY were wobbly and soft. The white scale bar at the bottom left is 3 cm.

incorporation of air bubbles (Figure 2, left and Figure S3a–c). This was to a much lesser degree observed with CA, LAC, T20, and T80 (Figure 2, right and Figure 3d–g). The pure film was a stable structure, able to stand alone and withstand light pressure when pressed by hand. In comparison to the films and crabs with additives though, it did not have any extraordinary stability or flexibility.

The addition of GLY resulted in a very soft and flexible film, which was easy to deform or break. The PEG hardened the material, but also made it more brittle. It was also shown in Figure S3c that it inherited some rips, making it even more brittle. SOR addition made it more flexible, without making it significantly harder or softer, while still incorporating a lot of small bubbles as visible in Figure S3b. With the addition of T20 and T80, the film was strengthened substantially so that they became harder than the pure film, but also more flexible. Additionally, they also gained a white sheen, while all the others stayed transparent. Finally, for LAC and CA the films behave very similarly: they are stronger, and LAC showed a high increase in flexibility, while CA showed a smaller increase in flexibility. This first observation is indicative of the potential applications of given plasticizers in chitosan-based products, as more flexible ones could be used as e.g., flexible film materials, while the more rigid ones could potentially find application as packing material, e.g., trays.

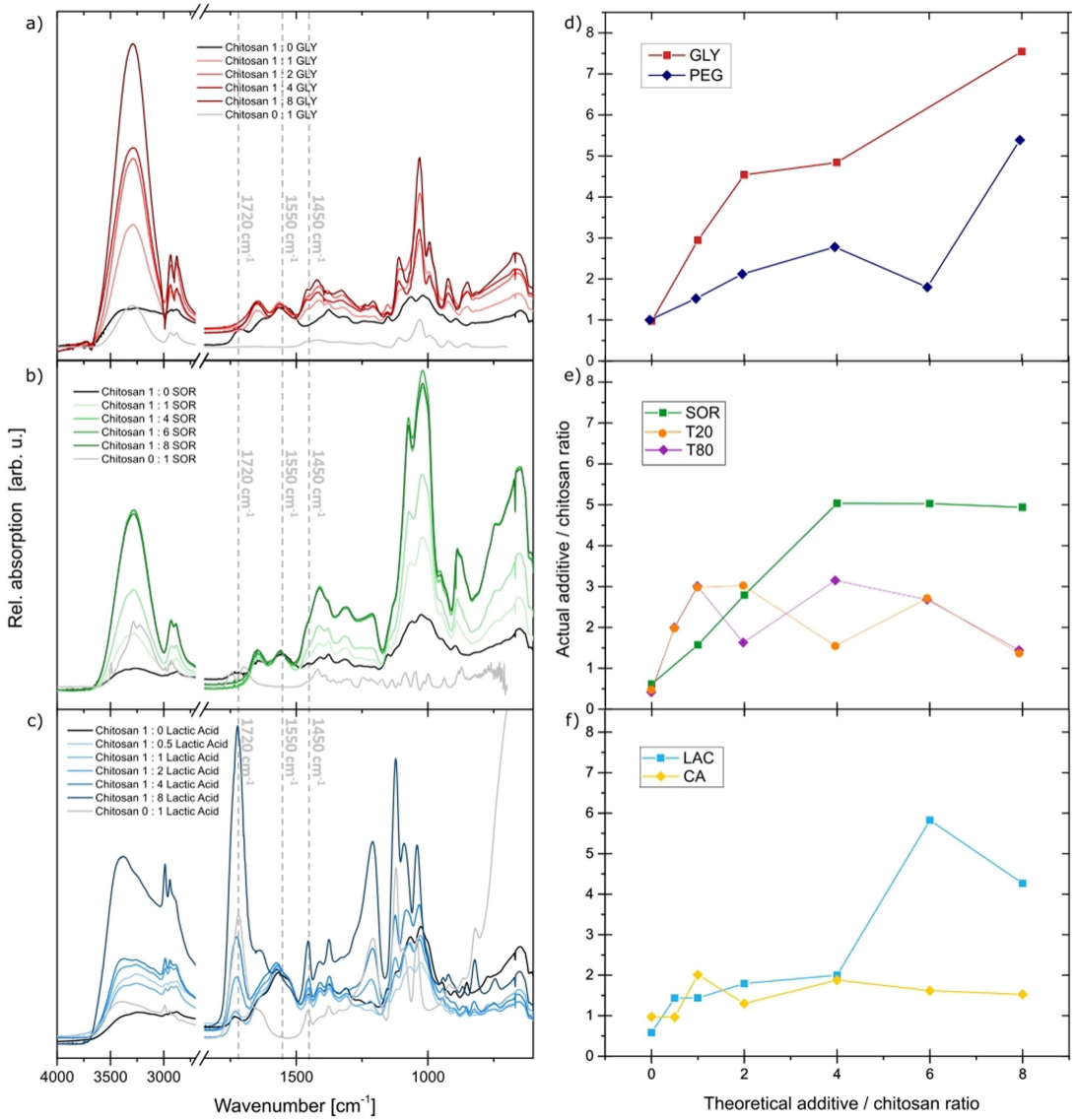

Figure 3. a–c): Attenuated total reflection infrared (ATR-IR) spectra of different additive to chitosan ratios from 0.5/1 (light colour) up to 8/1 (dark colour) of the additive glycerol (a; red), sorbitol (b; green), and lactic acid (c; blue). The pure chitosan spectrum is shown in all the Figures as a reference in black, the pure additive in light grey. With rising additive content, we see higher peaks corresponding to the additive for GLY, whereas we see a saturation for SOR, and a sudden jump for LA. All the spectra are normalized on the for chitosan specific N–H bend at 1550 cm^{-1}. In d–f) the ratios of an additive specific peak to the chitosan specific peak at 1550 cm^{-1} were plotted against the originally intended additive content. From here, the three earlier mentioned classes of additives become more obvious. In d) GLY (red; square) and PEG (dark blue; rhombus) show a linear correlation in additive uptake, while in e) for SOR (green; square), T20 (orange; circle), and T80 (violet; rhombus) a saturation behaviour can be seen at around 4/1 for all the additives. In f) we see a sudden jump and then stagnation of uptake for LAC (light blue; square) and CA (yellow; rhombus), which indicates a crosslink formed between the chitosan and the additive.

Attenuated total reflection-Infrared spectroscopy

For spectroscopic and microscopic analysis, films with different chitosan/additive (1/0.5 wt/wt up to 1/8 wt/wt) were mixed in solution and subsequently cast in a circular mould with a diameter of 2 cm on a glass substrate. After drying, the films were peeled off the glass. To examine the uptake of additive and its interaction with chitosan, ATR-IR spectra for all ratios are shown exemplarily for glycerol, sorbitol, and lactic acid in Figure 3. The equivalent IR spectra for the other additives are represented in Figure S4. As the amount of additive increases, their spectroscopic fingerprint increases in intensity as well. All spectra were normalized on the chitosan-specific N–H bending band at 1550 cm^{-1}, as none of the investigated additives has an intrinsic NH-moiety. Even if additives would be crosslinking the chitosan strands at this group, the N–H bending would not significantly be influenced, as an amide bond would be formed, which still has a characteristic N–H bending vibration at this position. Nevertheless, it was peak ratios that were compared, so as it was not calibrated before, the values given as the 'actual peak ratios' might be misleading. This holds not true for the trends received by the measurements though. Adding GLY as well as SOR (Figure 3a and 3b respectively) increases the

intensity of the bands around 3240 cm^{-1} and 1050 cm^{-1}, representing the O–H stretching and bending vibration, respectively.

With the addition of PEG (Figure S4a) many sharper bands arise in the spectra, mainly for the PEG characteristic C–H stretching (2800 cm^{-1}), C–H bending (1450 and 840 cm^{-1}), and C–O stretching (1280, 1220, and 1090 cm^{-1}) vibrations. T20 and T80 in Figure S4b and S4c respectively show with increasing additive amount a sharp increase in the C–H stretching at 2800 cm^{-1}, the C–O stretching at 1090 cm^{-1}, as well as the C–H bending (1450 and 840 cm^{-1}) vibrations. This is expected, as its structure visible in Figure S1 introduces a high amount of CH groups with the addition of the tweens. For increasing addition of LAC and CA, it is visible in Figure 3c and Figure S4d, respectively, that the O–H stretching (3380 cm^{-1}) and bending (1040 cm^{-1}) peaks increase in their intensity. Furthermore, the C=O stretching peak at 1720 cm^{-1} increases sharply with higher LAC and CA ratios, which makes sense as the spectra of the pure acids show C=O related peaks.

It is shown in Figure 3 and Figure S4 that for both GLY and PEG the peaks indicating the uptake of the additive increase steadily (though not perfectly linearly) from the ratios of additive to chitosan 0.5/1 up to 8/1. On the contrary, the spectra for SOR as well as T20 and T80 indicate an uptake maximum. This saturation is dependent on the additive used but seems to appear around a ratio of additive to chitosan 4/1 (Figure 3e). Furthermore, for LAC and CA, a slight shift in the peak at 1550 cm^{-1} towards higher wavenumbers is visible, indicating intermolecular interactions forming. The observed ratio of the two characteristic peaks does not change with increasing additive content up to a synthesis ratio of 4/1. This is likely due to saturation or crosslinking, also apparent from the appearance of additional OH-vibrations (3500–3000 cm^{-1}). The subsequent jump in the ratio might come from 'oversaturation' of the additive in the chitosan matrix, happening when the acids crosslinked with all NH_2 moieties of chitosan and then show in the spectrum themselves. This becomes even more apparent when looking at Figure 3d, 3e, and 3f, where the calculated ratios from the spectra in Figure 3 and Figure S4 are plotted against the initially prepared ratios. An additional note must be made about how the ratio of e.g., the LA was influenced by the fact that the 1550 cm^{-1} was actually more a shoulder band instead of a stand-alone peak, hence the found vs. theoretical additive/chitosan ratio might be lower in this specific case when determined using IR spectroscopy.

Pyrolysis gas chromatography coupled to mass spectrometry

Additionally, ATR-IR spectroscopy can be misleading in terms of additive saturation due to a limited probing depth, which means that a heterogeneous depth distribution of the additive might result in false saturation trends. To further validate that indeed certain additive/chitosan ratios saturate for increasing amounts, and to further study potential interactions between the additive and chitosan, Py-GC-MS was used. Here, the samples were pyrolyzed at 590 °C for 5 s and subsequently on-line injected on and measured with GC-MS.

In line with the ATR-IR spectroscopy measurements, pyrolysis of the films with additives could be classified in three groups: saturating, linear and indicative crosslinking, as shown in Figure 4 where representative fragment ions (found and motivated in the supporting information section C) of the additives are plotted against the amount of chitosan. Linear relationships between the amount of additive added and measured are observed for PEG and GLY. As seen in Figure 4a, PEG and GLY both clearly follow a linear trend with R2-values of 0.992 and 0.980, respectively. Note that the film-cast from an 8/1 ratio was not measurable for GLY, as it was very soft and sticky.

Another group of additives seemed to saturate at increasing ratios, as observed by ATR-IR spectroscopy. These are represented in Figure 4b. As can be seen for these three additives, they follow a non-linear increase. T20 and T80 were fitted to the plotted power-functions in Figure 4b with R^2-values of 0.999 and 0.993, respectively. Linear fits resulted in lower R^2-values

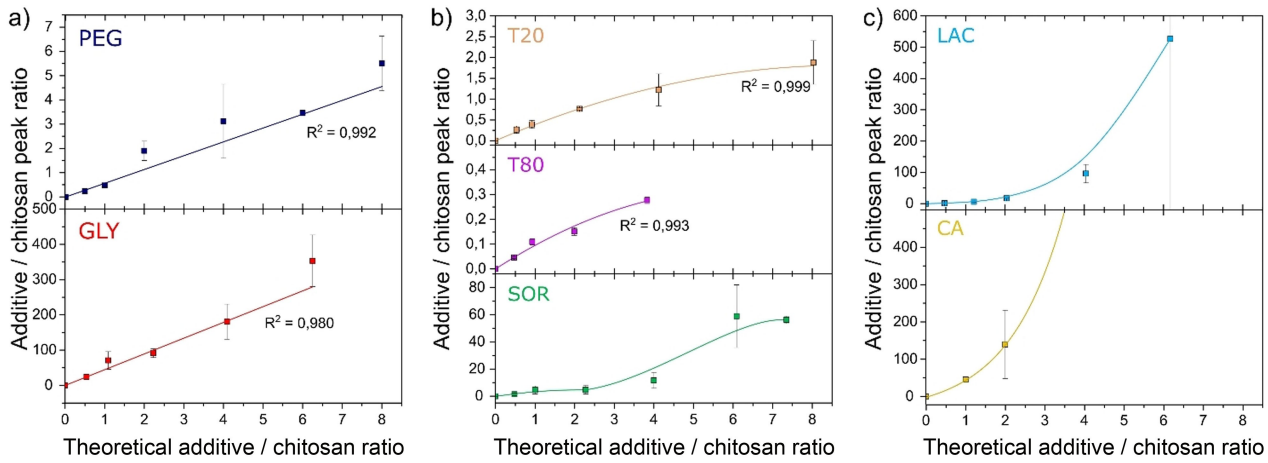

Figure 4. Correlations of the additive uptake and intended additive ratio in the formed chitosan films as deducted from pyrolysis gas chromatography coupled to mass spectrometry (Py-GC-MS) showing an a) non-saturating trend for PEG (dark blue; top) and GLY (red; bottom) b) saturating trend for T20 (orange; top), T80 (violet; middle), and SOR (green; bottom), and a c) crosslinking trend for LAC (light blue; top) and CA (yellow; bottom).

(0.997 and 0.988, respectively) indicating the saturation of the additive at higher ratios and confirming the observed trends using ATR-IR spectroscopy. For SOR, a rather gradual increase can be seen up until ratio 4/1, which is then followed by a jump and saturation for the higher ratios. In contrast to the five additives above that did not show any reaction products with chitosan, LAC and CA did. At low added amounts chitosan and chitin markers could still be identified, but at higher ratios their markers were absent. As a result, ratios of pyrolysis products from additives and those of chitosan and chitin markers became impossible to calculate for citric acid, while they increased exponentially for lactic acid (Figure 4c).

When LAC was used as an additive, the most prominent pyrolysis products generated included LAC itself, as an evaporation product, and lactide, as well as two compounds eluting closely after each other with a similar mass spectrum tentatively assigned as 'pyrazine–lactide' (the corresponding mass spectrum is shown in Figure S5). This tentative structure has a chiral centre, which explains why two peaks with an identical spectrum were observed. As control experiment, a 1/1 mixture of chitosan powder and LAC (without solvation and casting) was pyrolyzed and these two compounds were also observed. However, compared to the films containing LAC additive, the relative abundance was ≈1000 times higher in the latter implying during pyrolysis of the films these compounds probably represent a reaction product of chitosan with LA, at least from 0.5/1 to 4/1 mixtures. The 6/1 mixture showed a high variance of abundances of these two compounds, whereas for the 8/1 mixture these two isomers were hardly found with high abundances of both LAC and lactide. This is represented in Figure 5a, where the ratio of crosslinking product (pyrazine–lactide) and the chitosan marker (black) or the 'free' LAC marker (lactide in blue) is plotted. This shows that for the lower additive/chitosan ratios crosslinking dominates, which might induce a plastic-like effect. This fragment saturates above a ratio of 4/1, correlating to the steep jump found in Figure 4. Additional LAC does not crosslink anymore and could act as plasticizer in the resulting films. This means that the additive acts as a lubricant, sitting in between the polymer chains of the chitosan film, decreasing the intermolecular friction of the chitosan film and therefore decreases the hardness of the material and increases it flexibility.[44–46]

In case of CA, very prominent peaks were found for itaconic anhydride and/or citraconic anhydride, both generated upon pyrolysis of citric acid. During pyrolysis, two dehydration steps followed by decarboxylation take place.[47] Additionally, both the chitosan and chitin markers were hardly or not detected. Instead, a number of compounds, including three that have m/z 177 as the base peak or as second most abundant fragment ion were observed, and their relative abundance increased with increasing amount of citric acid added to chitosan upon pyrolysis. This product, represented in Figure 5b, follows a similar trend as seen for the LAC. The ratio of crosslinking product and chitosan (gold) increases infinitely as the chitosan unit was not observed anymore at ratios above 2/1. The crosslinking product decreases gradually, however, versus the free CA (black) showing the expected presence of CA as free additive and most likely as plasticizer, as all chitosan able to cross-link have been bound in the lower ratios. For both the LAC and CA, these steep 'jumps' in behaviour can also be found in the IR plots in Figure 3. LAC undergoes a strong increase after ratio 4/1, whereas CA increases after ratio 1/1 and stabilizes from ratio 2/1 onward.

Quantitative nanomechanical mapping

However, to measure how the addition of the different additives and their interactive behaviour with chitosan influences the resulting properties of the material, a physical interaction must be probed. Tensile testing, using a universal testing machine, is the most widely-applied technique to assess stress versus strain curves, giving the Young's modulus and elastic properties of the material (Figure S6a). To perform such measurements, 16×2 cm long strips were made for all additives (1/1 ratio to chitosan), as shown in Figure S6b, by slowly drying the casts in special moulds on a shaking plate. However, the strips did not have a homogeneous thickness, and this severely

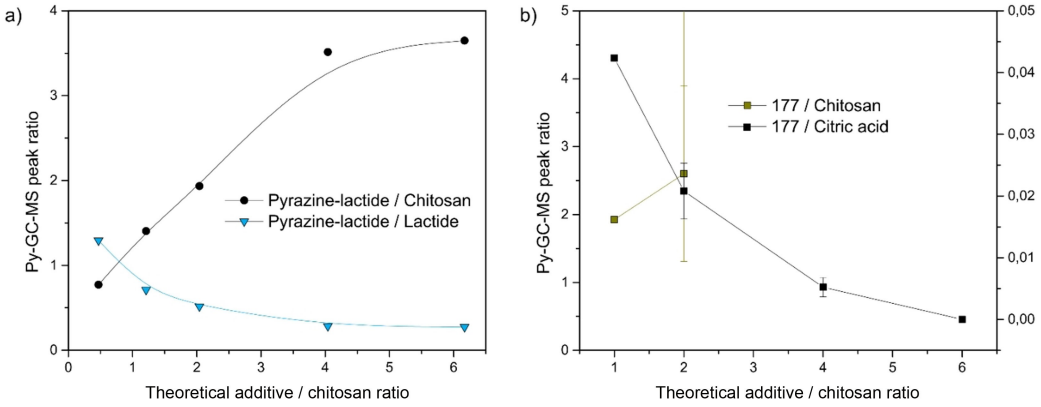

Figure 5. Pyrolysis gas chromatography coupled to mass spectrometry (Py-GC-MS) reveals cross-linking products which are plotted here against the chitosan or "free" additive as ratio for both a) LAC and b) CA, revealing that first the additive is taken up as cross-linking reagent, but then the chitosan sites are saturated and the further added additive will act as plasticizer in its free form.

impacted the tensile tests. Figure S6c shows the resulting stress versus strain curves, calculated for 10 thicknesses measured per strip (and the median was represented in the red curve). The variation in the resulting modulus is too large (factor 6 within the same sample) to draw strong conclusions, and not only will the thicknesses change these curves; it will not give a representative value for the product's material properties as the thinnest parts will act as weak-spots and rupture before the expected moment if the film would have had a perfect homogenous thickness.

However, to obtain the Young's modulus on a small sample, bypassing this problem and allowing us to study the physical properties of our chitosan-based films in a quantitative yet comparative method, we have utilized an AFM-derived technique to measure the surface of the films with different amounts of additives, as schematically shown in Figure 6a. Not only topological information was obtained, but the used mode (i.e., PeakForce mode) allowed the recording of force curves with high spatial resolution, which, after proper calibration, could be used to calculate physical properties such as adhesion, deformation, dissipation and stiffness (expressed using a DMT Young modulus), as shown in Figure 6b. This method is also referred to as quantitative nanomechanical mapping (QNM). In the approach taken in this work, sometimes referred to as the "relative calibration" method, a proper tip was calibrated on an "infinitely" strong and inflexible substrate, namely sapphire. Then we measured a pure chitosan film, which was always synthesized together with every batch of increasing amounts of plasticizers and used enough force to accumulate a deformation of 1–3 nm of the tip into the pure chitosan sample. The Young's modulus was tuned to be approximately 6–8 GPa, a value reported before for chitosan films.[48–51] These settings were not altered anymore, except the tip force, which was adjusted on every sample to always accumulate the same deformation, leading to a quantitative Young's modulus for the different additives and ratios to compare.

The resulting Young's modulus values are shown in Figure 6c–e, again classified per expected additive behaviour as done before for the ATR-IR and Py-GC-MS data. These values were determined from the full modulus maps scanned, which are shown in Figures S5–7. The values represent the median Young's modulus measured over the full map, and the error bars shown in Figure 6 represent the variation found in these maps. More details on the workflow and statistical relevance of

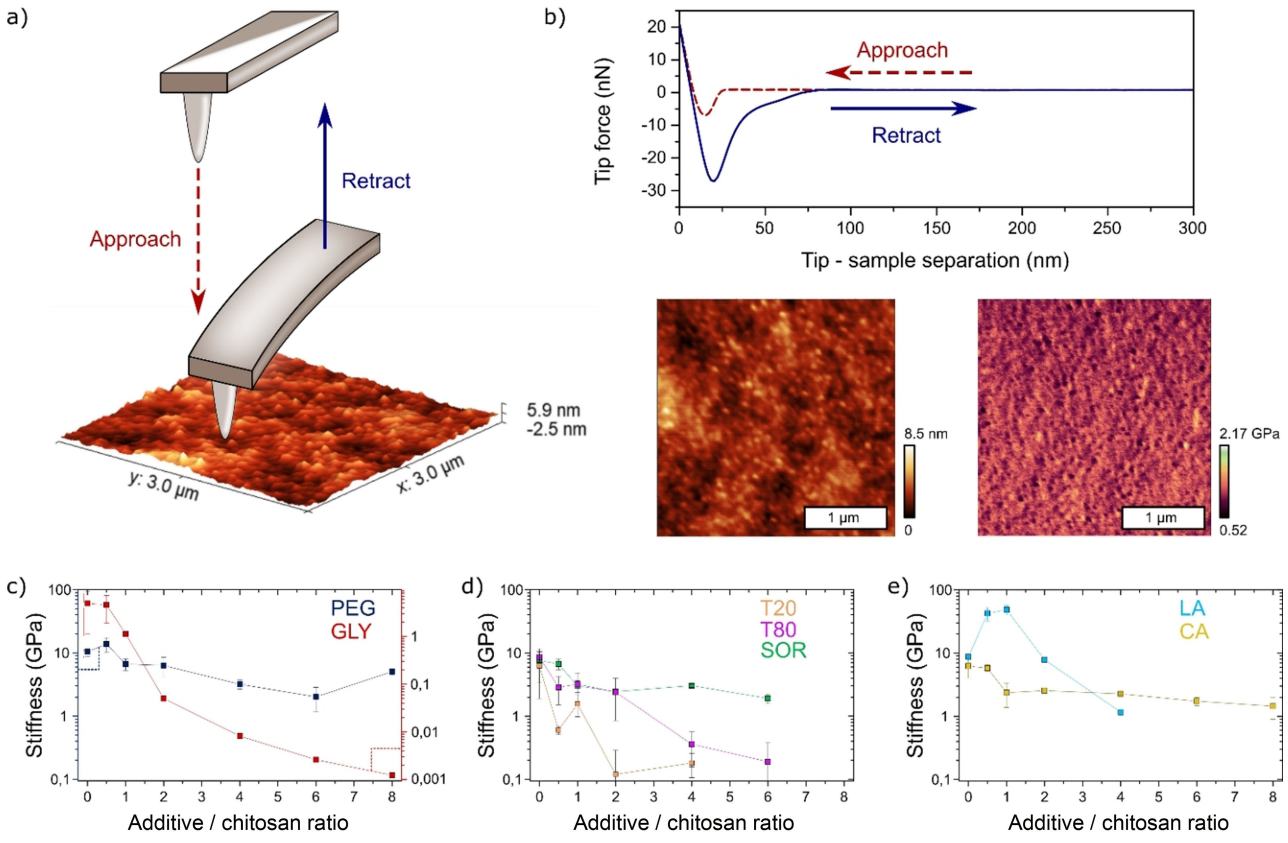

Figure 6. a) Atomic Force Microscopy (AFM) was used to perform quantitative nanomechanical mapping (QNM) on the different chitosan films, here showcased on a GLY/CHI 4/1 film. The tip is used as a calibrated spring to monitor the mechanical properties of the sample during approach and retraction of the tip. b) Resulting interactions are given in force curves, which can be used to calculated e.g., the Young's Modulus (E) at every specific location, which for this sample shows a homogeneous distribution. The stiffness defined using this approach were sorted again on c) non-saturating, d) saturating and e) cross-linking additives versus the increasing amount of additives. This reveals that GLY, T20, T80 and SOR act as plasticizers, whereas PEG forms a hybrid material with the chitosan itself. LAC and CA first cross-link increasing the stiffness of the resulting film, but then the free additive act as plasticizer making the resulting material softer. The error bars shown indicate the range of values found within one single modulus map per sample. The values plotted here can be found in Table S1 in the supporting information.

the QNM outcomes can be found in the Supporting Information. Interestingly, the Young's modulus of PEG seems to be rather constant with respect to the additive to chitosan ratio compared to the other additives. A slight decrease in stiffness is observed after the 0.5/1 ratio, but afterwards it seems similar. The PEG has a high molecular weight, and we expect that the GPa of PEG is close to that of chitosan. Hence, adding more PEG will not alter the resulting modulus too much if it does not act as plasticizer. The stiffness maps, shown in Figure S7 (non-saturating), Figure S8 (saturating) and Figure S9 (crosslinking), show the presence of an intertwining pattern of two different materials, hence we believe PEG indeed does not really serve as plasticizer but forms a hybrid-composite together with chitosan. This also explains the linear increase found in the ATR-IR spectroscopy and Py-GC-MS data.

In contrast for GLY, with increasing glycerol amount the stiffness decreases exponentially. We assume this is due to the fact that GLY acts as a plasticizer, which softens the chitosan film, but does not form locally fewer stiff domains on its own like PEG. Instead, the GLY fills the space between chitosan chains throughout the whole product, decreasing the intermolecular friction and hence decreasing the Young's modulus. In all utilized additives, the effects of GLY are the most pronounced. This is exemplified by the need to use a separate y-axis in Figure 6c to clearly display the evolution of the modulus over different amounts of additives. After adding 2 equivalents of GLY, the resulting material was already below 0.1 GPa, a value not found for any of the other additives. The stiffness could be even further decreased to ± 1 MPa, pushing it into a regime often found for rubbers. However, the workability and stability of the material was low as it would easily fracture at higher amounts of additive (GLY/CHI >4).

T20, T80, and SOR seem to saturate in the ATR-IR spectroscopy data, whereas in the Py-GC-MS data they showed a slight saturation, which was less pronounced. The stiffness (Figure 6d) reveals a rather linear decrease, at slightly saturating, which correlates to the amounts, as found for the Py-GC-MS data. This shows that the earlier saturation found for these additives is indeed due to a heterogeneous distribution of the additive on the surface vs. deeper in the material, which then leads to a saturating effect in the (limited) depth measured using ATR-IR spectroscopy. From this observation, we also expect that these materials serve as a plasticizer rather than a cross-linker or composite. Clear differences are found when comparing the additives. Sorbitol only has a minor effect on the resulting stiffness (going to a minimum of ± 2–3 GPa) compared to T20 and T80, which can bring the modulus of the resulting material as low as ± 0.2 GPa. After the addition of GLY, this is the lowest stiffness achieved for the chitosan films. T80 seemed to have less of a plasticizing effect per amount used compared to T20, reaching a lower resulting stiffness at lower amounts of additive.

The final group, as summarized in Figure 6c, categorized as crosslinking based on the ATR-IR spectroscopy and Py-GC-MS results, shows a different stiffness profile. With LAC stiffness increases with ratios up to 2/1, likely due to the crosslinking. However, at ratios above 2/1 a steep decay in stiffness is observed in line with the steep jump in Figure 5 observed with Py-GC-MS. The decrease in stiffness for ratios above 2/1 is likely due to the plasticizing effect of LAC not participating in crosslinking, as suggested before. This means that an excess LA sits between the chitosan as a lubricant, without actually being covalently bound to the polymer, while it lowers the intermolecular friction and further decreases the Young's modulus as a function of concentration. CA shows hardly any influence at low ratios, but as the content 'free' CA increases, as indicated by the ATR-IR spectroscopy, the stiffness drops, but then remains rather stable from ratio 1/1 onward and does not decrease significantly as was observed for LAC. Finally, we have further investigated the chitosan film cast with HCl in order to probe a stiffness difference, as visible in Figure S10. The film cast with HCl is a lot rougher than the film cast with acetic acid. Also, the stiffness of the chitosan film cast with acetic acid is higher (8.5 GPa mean value) in comparison to the film cast with HCl (3.9 GPa mean value), underlining further that reacetylation of the chitosan occurs upon drying when acetic acid is present.

All in all, these chitosan-based films show a broad range in their DMT-moduli (see Figure 6 and Table S1 in the supporting information), emphasizing how tunable they are with the right additives. This further makes them competitive to commercially available polymers, even though they appear more on the hard side, where the Young's moduli range from 0.2 GPa for low density polyethylene (LDPE) over 2.6 GPa for polycarbonate (PC), 3.0 for polystyrene (PS) up to 4.8 GPa for polymethyl methacrylate (PMMA).[52]

Grazing-incidence X-Ray diffractometry

In a next stage of our study, GI-XRD was used to study the crystalline properties of the chitosan-based films with additives (1/1 ratios) with the aim to evaluate their (semi−) crystallinity, potential crosslinking effects and the observed reacetylation. All XRD patterns were normalized to their highest reflex (at around 20°). The XRD patterns, shown in Figure 7, indicate three major reflections visible at $\approx 9°$ (020), $\approx 13°$, and $\approx 20°$ (110) (exact values found in Table S2 in the supporting information).[53,54] According to literature, the two XRD peaks at $\approx 9°$ (020) and $\approx 20°$ (110) are indicative of the degree of acetylation, with an increased peak intensity being representative of a high degree of acetylation.[53,54] The XRD peak at $\approx 13°$ is intrinsic to the *N*-acetylated nature of chitosan.[54] Figure 7a shows the chitin polymer in red, the chitosan polymer in grey, and the chitosan film in black, which shows an additional third reflex to the chitosan polymer at $\approx 13°$, indicative of reacetylation. Pure chitosan, CA, as well as LAC, show the presence of all three XRD peaks, while most of the other additives are missing the second one at $\approx 13°$. Whereas for pure chitosan this indicates reacetylation, CA and LAC are shown to undergo crosslinking and yielding more (semi−) crystallinity in the process. Furthermore, the X-ray diffractogram of chitin shows a clear splitting of the peak at $\approx 20°$.[53,54]

As a final confirmation to show that our synthesis procedure leads to the reacetylation of the utilized chitosan feedstock, we

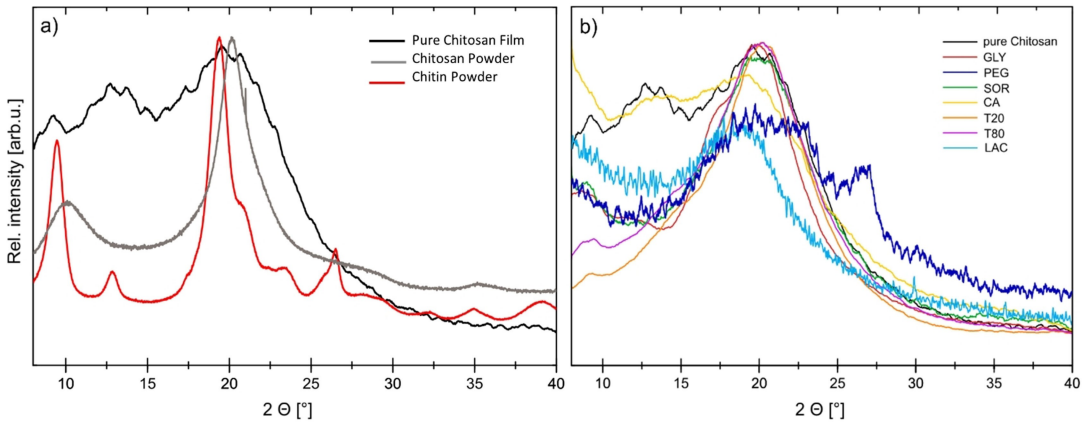

Figure 7. a) Grazing-Incidence X-Ray Diffraction (GI-XRD) pattern of a pure chitosan film (black, top line) and Bragg's mode X-Ray Diffraction (XRD) patterns of chitin powder (red, bottom line) and chitosan powder (grey, middle line) as reference. The pure chitosan film shows additionally to the two reflexes of the chitosan powder at ≈9° (020) and ≈20° (110) a third one at ≈13°, which is at the same angle as the chitin powder reflex. b) GI-XRD patterns of the pure chitosan film (black) and of chitosan with the additives PEG (dark blue), GLY (red), SOR (green), T20 (orange), T80 (violet), LAC (light blue), and CA (yellow) in a 1/1 ratio. Next to the two main peaks at ≈9° (020) and ≈20° (110), crosslinking additives show a third peak arising at ≈13° which is indicative of some form of acetylation at the NH moiety of the chitosan. All diffractograms are normalized.

have measured the thermal stability of the films cast with 1 wt.% HCl or 1 wt.% acetic acid. For HCl, this corresponds to 10.0 g/L or 274 mmol/L, while for acetic acid this corresponds to 10.0 g/L or 167 mmol/L. The Thermal Gravimetric Analysis (TGA) profile (Figure S11) demonstrates that the films cast with acetic acid are stable at higher temperatures. When cast with acetic acid, the film withstands up to a temperature of around 276 °C, whereas the film cast with HCl already degraded at around 213 °C. This further confirms the increased strength of our cast film due to the reacetylation, having potentially large impacts on using chitosan as a feedstock for applications in which stronger, sturdier plastics are aimed to be replaced, i.e., packaging material. Additionally, one could imagine that the reacetylation could be tuned leading to a more rational design of the chitosan-based casts, in which the additives presented in this work then provide even more options in terms of physical properties for the final products.

Conclusion and Future Perspectives

With the introduction of green additives, it is possible to induce a broad variety of physical properties to the chitosan-based 'plastic' films. All seven additives under study, namely glycerol (GLY), sorbitol (SOR), polyethylene glycol (PEG), lactic acid (LAC), citric acid (CA), Tween 20 (T20), and Tween 80 (T80), form a smooth, flat, and shapable film when cast and dried with a 1/1 additive-to-chitosan ratio. When assessing the uptake behaviour of the additives into the chitosan matrix using ATR-IR spectroscopy (Figure 3) and Py-GC-MS analysis (Figure 4), we did not obtain net additive/chitosan mass ratios, but instead coherently found that additives will follow either a linear uptake, a non-linear uptake, or a crosslinking one as their either more surface-dependent interaction or crosslinking behaviour became discernible using the combination of these analytical techniques. For all additives under study, it can be said that lower ratios (1/1 and lower) are the most promising for practical applications as the respective physical properties are well affected by the additive, while still maintaining a good mechanical stability.

Linearly integrated additives (i.e., GLY, and PEG) show a full uptake of the additive even at high additive to chitosan ratios. Nevertheless, they become mechanically unstable and unpractical to handle at higher additive-to-chitosan ratios (GLY becomes too jelly, working as a plasticizer, while PEG forms a hybrid-composite and becomes too brittle). No interaction between the additives and the chitosan with linearly incorporated additives was observed.

Instead, SOR, T20, and T80 show an uptake maximum of the additive at around a ratio of about 4/1. Nevertheless, a shift in the saturating ratio is observed between the more outer-layer sensitive ATR-IR spectroscopy results and the full-sample Py-GC-MS measurements, indicating additives being incorporated heterogeneously over the film thickness. All these additives do not interact with chitosan, leading to the conclusion that additives structurally and chemically similar to chitosan have a maximum uptake while acting as plasticizer. LAC and CA introduce crosslinking up to a 1/1 ratio, but at even higher ratios the "extra" additives act as a plasticizer as well. In parallel, reacetylation of the pure chitosan film is observed when dissolved and casted from the acetic acid solution, which can have large implications in the application of pure chitosan films itself, as it regains some of the structural stability and strength that chitin is praised for.

Hence, we have shown that a variety of green additives can facilitate the formation of stable chitosan-based 'plastic' products, ranging from soft and flexible to hard and sturdy materials. Adding varying additives into bio-based plastics increases their potential field of applications, ranging from cling-film like materials to e.g., hard trays, making them an even more promising alternative to fossil fuel-based plastics. Furthermore, they become competitive with commercially available plastics in their stiffness and flexibility with some of the studied bio-

based additives. This broad comparison of green additives and their effect on the chitosan films aims to help directing and steering the properties of chitosan-derived materials in a systematic manner, lowering the barrier to utilize it in a broader scale.

However, before being completely viable for industrial application and being transferrable to other biomass resources, some challenges still need to be tackled: The methodology shown here to cast and study such bio-plastics can be applied to other biopolymers and additives alike, and QNM specifically could be pushed to even gain information on the integrity of the films on the nanoscale while bringing an alternative to tensile tests for materials still being developed on a small, lab-based scale. We suggest that future research further should thoroughly discuss thermal and mechanical properties of the industrially viable films, as well as track those over a substantial period to look at their aging behaviour. This will help to understand both the processing range of the materials, as well as the thermal stability.

Additionally, research including fungal-derived chitosan, which is easier controllable in molecular weight and degree of acetylation would be of high interest, in order to compare the physical chemical properties of those materials. Like this, it could be potentially even possible to link the structure of the chitosan with properties of the final material, giving researchers and industries alike insights and a handle on how to tune not only chitosan-derived films, but potentially even in general biomass-derived materials.

Experimental Section

Film formation

All films were made with a 1 wt.% chitosan (98% purity, $\geq$75% deacetylated, Sigma-Aldrich) solution in 1 wt.% acetic acid ($\geq$99%, glacial, ReagentPlus®, Sigma-Aldrich)/water solution. The chitosan was dissolved overnight under stirring at room temperature. Afterwards, glycerol (GLY; Sigma-Aldrich, $\geq$99%), sorbitol (SOR; Sigma, $\geq$98%), polyethylene glycol (PEG; Merck, for synthesis, 20000 g mol^{-1}), lactic acid (LAC; Fluka Analytical), citric acid (CA; Sigma-Aldrich, 99%), Tween 20 (T20; Sigma-Aldrich, for synthesis), and Tween 80 (T80; Sigma-Aldrich, for synthesis) were added in wt. ratios of 0.5, 1, 2, 4, 6 and 8 and left to stir for another night. 2 mL of the mixture was dispersed into a mould of 2 cm in diameter on a glass plate. The moulds were air dried for 48 h up to 72 h. After drying, the films were taken as they were and not washed or treated before measuring. For the tensile tests, larger moulds of 16×2 cm were used with 40 mL of synthesis solution and shaken during the drying process at 50 rpm.

Attenuated total reflection-Infrared spectroscopy

Attenuated total reflection-infrared (ATR-IR) spectroscopy was recorded on a Perkin Elmer Frontier spectrometer with a $LiTaO_3$ detector. The spectra were recorded from 600 to 4000 cm^{-1} averaged over 32 scans with a resolution of 2 cm^{-1}. The spectra were post-processed using an automatic background correction from the Perkin Spectrum software.

Pyrolysis gas chromatography coupled to mass spectrometry

Pyrolysis was carried out on a Horizon Instruments Curie-Point Pyrolyzer instrument. Samples (typically 0.5–1 mg) were pressed onto Ni/Fe Curie point wires and subsequently heated for 5 s at 590 °C. The pyrolysis unit was directly connected to a Carlo Erba GC8060 gas chromatograph (GC) and the reaction products were separated by a fused silica column (Agilent J&W CP8922, 25 m, 0.32 mm i.d.) coated with VF-1 ms (film thickness of 0.40 μm). He was used as carrier gas. The GC column was directly connected to the pyrolysis unit through a splitless injector set at 280 °C. The oven was initially kept at 40 °C for 1 min, next it was heated at a rate of 7 °C min^{-1} to 320 °C and maintained at that temperature for 15 min. The column was coupled to a Fisons MD800 mass spectrometer (MS) (mass range *m/z* of 45–650, ionization energy of 70 eV, and cycle time of 0.7 s). Each sample was measured 2–4 times, hence the error bars in Figures 4 and 5 in the main manuscript express the variance.

Atomic force microscopy

Atomic Force Microscopy (AFM) was measured utilizing a Bruker MultiMode8 instrument with J scanner and RTESPA antimony-doped silicon tips. The films were attached with copper tape to a magnet and then mounted on the AFM stage. For measurements on PEG, T20 and T80, the tips were used with a resonance frequency of 525 kHz and a spring constant of 200 N m^{-1}, whereas for GLY, CA, LA and SOR the tips were used with a resonance frequency of 150 kHz and a spring constant of 5 N m^{-1}. To measure the stiffness, quantitative nanomechanical mapping (QNM) mode was used. First, the tips were calibrated on a sapphire sample. Using a "relative" calibration approach, the tips were then used to measure a pure chitosan film and adjust the calculated DMT modulus between 6 and 8 GPa. Afterwards, the films with increasing amount of plasticizer were measured on a 3×3 μm area, 512×512 pixels, similar as has been reported by Sokolova et al.[51] yes its okay For every plasticizer, the different samples with increasing amount of additive were measured in the same run, using the same tip and same calibrated settings. The AFM micrographs were post-treated using Gwyddion. First, a planar background subtraction was performed, followed by a line-by-line correction using a trimmed mean-of-differences function. For the stiffness maps, only the line-by-line correction was performed. Outliers for the stiffness were masked ($>$20 GPa) and not taken into account by determining the median stiffness, which was found using the statistical quantities function of the software. The "error bars" depicted in the main manuscript represent the root-mean square values found for the stiffness recorded over the full ROI. Hence, the error bars reflect the homogeneity of the spots measured per sample. For all measurements, these error bars were found to be relatively small confirming proper measurements and homogeneity of the films. However, to clarify, the error bars do not indicate homogeneity over the full sample outside the assessed spot per sample.

Grazing incidence X-ray diffraction

The grazing incidence X-ray diffraction (GI-XRD) measurements of the films were carried out on a Bruker D8 Discover XRD instrument with grazing-incidence (GI) angle module. The films were stuck with a copper tape flat on a commercial XRD sample holder. Then they were measured for 40 h at 0.3°θ under static conditions from 5 to 40° 2θ with 40 kV and a current of 40 mA with a Cu tube.

Thermogravimetric analysis

A Perkin Elmer 8000 instrument was used for performing Thermogravimetric Analysis (TGA). Under N_2 atmosphere the sample was heated to 150 °C at 10 °C min^{-1}. After that, the heating ramp was adapted to 5 °C min^{-1} from 150 °C up to 1000 °C, where the atmosphere was switched to O_2 and held for 10 min to burn off the remaining rest of the sample.

Tensile tests

A Lloyd Tensile tester LS5 universal testing machine was used to load the 16×2 cm strips in 2 clamps, producing stress versus strain curves as the strips were pulled with 2 cm min^{-1} with a 1 kN head.

Supplementary Data

Information associated with this article can be found in the Supporting material. Additional references have also been cited within the Supporting Information (Ref. [55–74]).

Acknowledgements

This work was supported by the Advanced Research Center Chemical Building Blocks Consortium (ARC CBBC), founded by AkzoNobel, BASF, Nouryon and Shell and the universities of Eindhoven, Groningen and Utrecht with the support of the Netherlands Organization for Scientific Research (NWO). Additional funding comes from The Netherlands Center for Multiscale Catalytic Energy Conversion (MCEC), an NWO Gravitation program funded by the Ministry of Education, Culture and Science of the government of The Netherlands.

Conflict of Interests

The authors declare no conflicts of interest.

Data Availability Statement

The data that support the findings of this study are available from the corresponding author upon reasonable request.

Keywords: Chitosan · Bioplastics · Film Formation · Atomic Force Microscopy · Infrared Spectroscopy

[1] M. Yadaf, P. Goswami, K. Paritosh, M. Kumar, N. Pareek, V. Vivekanand, *Bioresour. Bioprocess.* **2019**, *6*, 8.
[2] G. Beall, "By Design: World War II, plastics, and NPE", can be found under http://www.plasticstoday.com/imm/articles/design-world-war-ii-plastics-and-npe, **2009** (accessed October 10, 2022).
[3] University of Georgia, "More than 8.3 billion tons of plastics made: Most has now been discarded", can be found under http://www.sciencedaily.com/releases/2017/07/170719140939.htm, **2017** (accessed October 10, 2022).
[4] PlascticsEurope. "Plastics – the Facts 2020: An analysis of European plastics production, demand and waste data", can be found under https://issuu.com/plasticseuropeebook/docs/plastics_the_facts-web-dec2020, **2020** (accessed July 31, 2023).
[5] I. Vollmer, M. J. F. Jenks, M. C. P. Roelands, R. J. White, T. van Harmelen, P. de Wild, G. P. van der Laan, F. Meirer, J. T. F. Keurentjes, B. M. Weckhuysen, *Angew. Chem. Int. Ed.* **2020**, *59*, 15402–15432.
[6] A. Shrotri, H. Kobayashi, A. Fukuoka, *Adv. Catal.* **2017**, *60*, 59–123.
[7] J. R. Jambeck, R. Geyer, C. Wilcox, T. R. Siegler, M. Perryman, A. Andrady, R. Narayan, K. L. Law, *Sci.* **2015**, *347*, 1655–1734.
[8] P. Cazón, G. Velazquez, J. A. Ramírez, M. Vázquez, *Food Hydrocolloids* **2017**, *68*, 136–148.
[9] P. Cazón, G. Velazquez, *Sustain. Agric.* **2019**, *36* 81–123.
[10] Á. Molnár, *Coord. Chem. Rev.* **2019**, *388*, 126–171.
[11] J. Zakzeski, P. C. A. Bruijnincx, A. L. Jongerius, B. M. Weckhuysen, *Chem. Rev.* **2010**, *110*, 3552–3599.
[12] M. Rinaudo, *Prog. Polym. Sci.* **2006**, *31*, 603–632.
[13] T. Huq, A. Khan, D. Brown, N. Dhayagude, Z. He, Y. Ni, *J. Biores. Bioprod.* **2022**, *7*, 85–98.
[14] I. S. Arvanitoyannis, A. Kassavet, *Int. J. Food Sci. Technol.* **2008**, *43*, 726–745.
[15] M. G. Healy, C. R. Romo, R. Bustos, *Resour. Conserv. Recycl.* **1994**, *11*, 139–147.
[16] G. S. Dhillon, S. Kaur, S. Brar, M. Verma, *Crit. Rev. Biotechnol.* **2013**, *33*, 379–403.
[17] K. Mohan, A. R. Ganesan, P. N. Ezhilarasi, K. K. Kondamareddy, D. K. Rajan, P. Sathishkumar, J. Rajarajeswaran, L. Conterno, *Carbohydr. Polym.* **2022**, *287*, 119349.
[18] Y. Xu, M. Bajaj, R. Schneider, S. L. Grage, A. S. Ulrich, J. Winter, C. Gallert, *Microb. Cell Fact.* **2013**, *12*, 90.
[19] L. Wie, W. Deng, S. Li, Z. Wu, J. Cai, J. Luo, *J. Biores. Bioprod.* **2022**, *7*, 63–72.
[20] I. Younes, M. Rinaudo, *Mar. Drugs* **2015**, *13*, 1133–1174.
[21] M. Aider, *LWT-Food Sci. Technol.* **2010**, *43*, 837–842.
[22] S. Hemjinda, A. Krzan, E. Chiellini, S. Miertus in *Environmentally Degradable Polymeric Materials and Plastics – Guidelines to Standards and Testing Practices*, **2007**, 36.
[23] ScienceDirect, can be found under http://www.sciencedirect.com/search?qs=chitosan%20film&years=2017%2 C2016%2 C2018%2 C2019%2 C2020&lastSelectedFacet=years (accessed September 24, 2021).
[24] Unitika Inc., "100 Years of Unitika", can be found under http://www.unitika.co.jp/company/archive/history/ (accessed September 24, 2021).
[25] Hemostasis, "Elevating Patient Care Through Collaboratice Innovation", can be found under http://www.hemostasisllc.com/products/ (accessed September 24, 2021).
[26] Y. X. Wang, H. Ishida, *Polym. Sci.* **2002**, *86*, 2953–2966.
[27] N. V. Majeti, R. Kumar, *React. Funct. Polym.* **2000**, *46*, 1–27.
[28] N. E. Suyatma, L. Tighzert, A. Copinet, V. Coma, *J. Agric. Food Chem.* **2005**, *53*, 3950–3957.
[29] M. A. Da Silva, A. Krause Bierhalz, T. G. Kieckbusch, *Carbohydr. Polym.* **2009**, *77*, 736–742.
[30] A. D. Godwin, in *Applied Plastics Engineering Handbook: Processing, Materials: and Application, Elsevier*, Amsterdam, **2016**.
[31] K. Ziani, J. Oses, V. Coma, J. I. Maté, *LWT-Food Sci. Technol.* **2008**, *41*, 2159–2165.
[32] M. M. Sabet, T. M. Tamer, A. M. Omer, W. M. Salem, M. A. Hassan, M. H. Gouda, S. M. Eldin, *Egypt. J. Chem.* **2020**, *63*, 1989–1998.
[33] N. A. Imani, M. Kusumanigrum, *Chemica: Jurnal Teknik Kimia* **2019**, *6*, 77.
[34] K. Ziani, J. Oses, V. Coma, J. I. Maté, *LWT-Food Sci. Technol.* **2008**, *41*, 2159–2165.
[35] T. S. Parreidt, M. Schott, M. Schmid, K. Müller, *Int. J. Mol. Sci.* **2018**, *19*, 1–21.
[36] M. G. A. Vieira, M. A. Da Silva, L. O. Dos Santos, M. M. Beppu, *Eur. Polym. J.* **2011**, *47*, 254–263.
[37] M. Liu, Y. Zhou, Y. Zhang, C. Yu, S. Cao, *Food Hydrocolloids* **2013**, *33*, 186–191.
[38] M. G. N. Campos, L. H. I. Mei, A. R. Santos, *Mater. Res.* **2015**, *18*, 781–790.
[39] W. H. Jiang, S. J. Han, *J. Polym. Sci. Part B* **1998**, *36*, 1275–1281.
[40] I. C. Pereira, A. S. Duarte, A. S. Neto, J. M. F. Ferreira, *Mater. Sci. Eng. C* **2019**, *96*, 606–615.
[41] J. Khouri, A. Penlidis, C. Moresoli, *Processes.* **2019**, *7*, 157.
[42] S. Girdthep, W. Punyodom, R. Molloy, W. Channuan, in *International Conference on Chemistry and Chemical Process*, **2011**, *10*, 95–100.

[43] I. Arzate-Vazquez, J. J. Chanona-Perez, G. Calderon-Dominquez, E. Terres-Rojas, V. Garibay-Febles, A. Martínez-Rivas, G. F. Gutiérrez-López, *Carbohydr. Polym.* **2012**, *87*, 289–299.
[44] A. D. Godwin, in *Applied Plastics Engineering Handbook: Processing, Materials, and Applications*, William Andrew Publishing: Amsterdam, **2016**, pp. 533.
[45] F. W. Clark, *Chem. Ind.* **1941**, *60*, 225–230.
[46] D. F. Cadogan, C. J. Howick, in *Plasticizers. Kirk-Othmer Encyclopedia of Chemical Technology; John Wiley and Sons*. New York, **1996**.
[47] D. Wyrzykowski, E. Hebanowska, G. Nowak-Wiczk, M. Makowski, L. Chmurzyński, *J. Therm. Anal. Calorim.* **2011**, *104*, 731–735.
[48] H. Wu, Y. Lei, J. Lu, R. Zhu, D. Xiao, C. Jiao, R. Xia, Z. Zhang, G. Shen, Y. Liu, S. Li, M. Li, *Food Hydrocolloids* **2019**, *97*, 105208.
[49] H. R. Le, S. Qu, R. E. Mackay, R. Rothwell, *J. Adv. Ceram.* **2012**, *1*, 66–71.
[50] A. Aryaei, A. H. Jayatissa, A. C. Jayasuriya, *J. Mech. Behav. Biomed. Mater.* **2012**, *5*, 82–89.
[51] M. P. Sokolova, M. A. Smirnov, A. A. Samarov, N. V. Bobrova, V. K. Vorobiov, E. N. Popova, E. Filippova, P. Geydt, E. Lahderanta, A. M. Toikka, *Carbohydr. Polym.* **2018**, *197*, 548–557.
[52] T. J. Young, M. A. Monclus, T. L. Burnett, W. R. Broughton, S. L. Ogin, P. A. Smith, *Meas. Sci. Technol.* **2011**, *22*, 125703.
[53] Y. Zhang, C. Xue, Y. Xue, R. Gao, X. Zhang, *Carbohydr. Res.* **2005**, *340*, 1914–1917.
[54] A. V. Raut, R. K. Satvekar, S. S. Rohiwal, A. P. Tiwari, A. Gnanamani, S. Pushpavanam, S. G. Nanaware, S. H. Pawar, *Des. Monomers Polym.* **2016**, *19*, 445–455.
[55] B. A. Stankiewicz, P. F. van Bergen, I. J. Duncan, J. F. Carter, D. E. Briggs, R. P. Evershed, *Rapid Commun. Mass. Spectrom.* **1996**, *10*, 1747-1757.
[56] L. Zheng, C. Qin, L. Wang, W. Li, *Carbohydr. Polym.* **2011**, *83*, 1553–1557.
[57] Z. Lin, T. Wang, X. Han, D. Han, S. Li, *J. Anal. Appl. Pyrolysis* **2008**, *81*, 121–126.

Manuscript received: April 24, 2023
Revised manuscript received: August 5, 2023
Accepted manuscript online: August 7, 2023
Version of record online: September 5, 2023